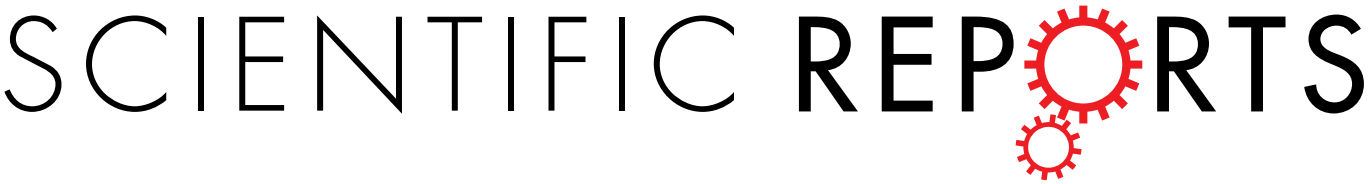

OPEN

Voltage-induced magnetization dynamics in CoFeB/MgO/CoFeB magnetic tunnel junctions

Received: 12 September 2016
Accepted: 10 January 2017
Published: 17 February 2017

Katsuya Miura[1,2], Shin Yabuuchi[1], Masaki Yamada[1], Masahiko Ichimura[1], Bivas Rana[2], Susumu Ogawa[1], Hiromasa Takahashi[1], Yasuhiro Fukuma[2,3] & Yoshichika Otani[2,4]

Recent progress in magnetic tunnel junctions (MTJs) with a perpendicular easy axis consisting of CoFeB and MgO stacking structures has shown that magnetization dynamics are induced due to voltage-controlled magnetic anisotropy (VCMA), which will potentially lead to future low-power-consumption information technology. For manipulating magnetizations in MTJs by applying voltage, it is necessary to understand the coupled magnetization motion of two magnetic (recording and reference) layers. In this report, we focus on the magnetization motion of two magnetic layers in MTJs consisting of top layers with an in-plane easy axis and bottom layers with a perpendicular easy axis, both having perpendicular magnetic anisotropy. According to rectified voltage (V_{rec}) measurements, the amplitude of the magnetization motion depends on the initial angles of the magnetizations with respect to the VCMA direction. Our numerical simulations involving the micromagnetic method based on the Landau-Lifshitz-Gilbert equation of motion indicate that the magnetization motion in both layers is induced by a combination of VCMA and transferred angular momentum, even though the magnetic easy axes of the two layers are different. Our study will lead to the development of voltage-controlled MTJs having perpendicular magnetic anisotropy by controlling the initial angle between magnetizations and VCMA directions.

Electron-spin-related phenomena have been attracting much attention because of their potential for enabling innovation in information processing technologies such as magnetic random access memory (MRAM)[1–3] and nonvolatile logic chips. The essential technology to enable such innovation is manipulating magnetizations with low power consumption, which can contribute to sustainable green information technology world. Spin-transfer torque (STT)[4,5] induced by spin-polarized current or magnetic (Oersted) fields[6,7] induced by charge current are conventionally used to manipulate or switch magnetizations. However, power consumption cannot be reduced beyond a certain level for the current-controlled manipulation of magnetizations due to inherent Joule heating.

In addition to STT magnetization switching, the discovery of perpendicular magnetic anisotropy (PMA) at the interface between CoFeB and MgO[8,9], which are widely used in magnetic tunnel junctions (MTJs)[8–12] due to their giant tunnel magnetoresistance (TMR)[13], is substantial progress in developing practical MRAM. To further reduce power consumption, many different trials for manipulating magnetic properties by voltage have been conducted, including voltage control of magnetostriction in multilayered stacks with piezoelectric materials[14,15], Currie temperature in ferromagnetic semiconductors[16,17], magnetoelectric effect in multiferroic materials[18] or ferroelectric/ferromagnetic heterostructures[19], and magnetic anisotropy[20,21].

It has recently been reported that the ferromagnetic resonance (FMR) in MTJs with a perpendicular magnetic easy axis to the plane (p-MTJs) can be induced by applying radio frequency (RF) voltage due to voltage-controlled magnetic anisotropy (VCMA)[22–26]. Thus, the power consumption in MRAM can be significantly reduced if magnetizations in MTJs are fully controlled by applying voltage.

To develop voltage-controlled MTJs, the coupled motion of two magnetizations in MTJs must be considered because MTJs have two magnetic layers (recording and reference) and those two magnetizations are coupled to each other through interlayer dipolar coupling. To understand the magnetization motion in the two

[1]Research and Development Group, Hitachi, Ltd., 1-280 Higashi-koigakubo, Kokubunji-shi, Tokyo 185-8601, Japan. [2]Center for Emergent Matter Science, RIKEN, 2-1 Hirosawa, Wako 351-0198, Japan. [3]Frontier Research Academy for Young Researchers, Kyushu Institute of Technology, 680-4 Kawazu, Iizuka 820-8502, Japan. [4]Institute for Solid State Physics, University of Tokyo, Kashiwa 277-858, Japan. Correspondence and requests for materials should be addressed to K.M. (email: katsuya.miura.aq@hitachi.com)

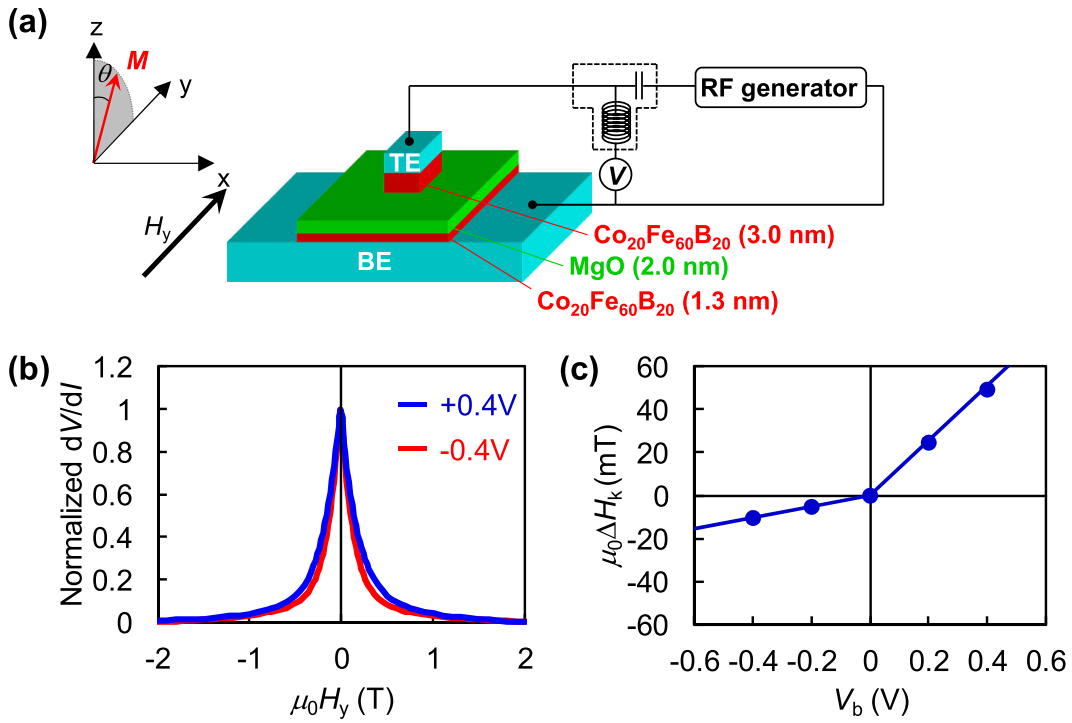

Figure 1. Schematic representation of sample structure and experimental results of VCMA magnitude. (**a**) Schematic illustration of CoFeB/MgO-based MTJ structure used in this study and experimental setup for rectified voltage measurements. (**b**) Normalized dV/dI as function of H_y under $|V_b| = 0.4$ V. (**c**) Dependence of $\mu_0 \Delta H_k$ on V_b, from which we obtain $\mu_0 \Delta H_k / V$ of 127.1 (26.0) mT/V in positive (negative) V_b region.

magnetic layers under applied voltage, we conduct rectified voltage (V_{rec}) measurements[27,28] in MTJs that have a relatively thicker top CoFeB layers with an in-plane magnetic easy axis and ultrathin bottom CoFeB layers with a perpendicular magnetic easy axis[8], and conduct numerical micromagnetic simulations based on the Landau-Lifshitz-Gilbert (LLG) equation of motion by taking into account VCMA on a model sample consisting of two CoFeB layers.

Results and Discussion

We prepare MTJs having 3-nm-thick top CoFeB layers (reference layer) with the in-plane magnetic easy axis and 1.3-nm-thick bottom CoFeB layers (free layer) with the perpendicular magnetic easy axis[8] (see Methods), as schematically shown in Fig. 1(a), along with the coordinate system. The CoFeB layers are separated by a 2.0-nm-thick MgO layer.

The reason for having PMA in the thin CoFeB layers has been attributed to the hybridization of Fe 3*d* and O 2*p* orbitals from the first-principles calculation[29]. The basic idea of VCMA is the modulation of the charge or spin density in the 3*d* orbitals by voltage or electric field[30–32]. Relative changes in spin density in the occupied orbitals can cause a change in PMA.

Both (top and bottom) ferromagnetic layers in our MTJs have interfacial PMA because they have an interface with the MgO layer. However, the direction of the easy axis strongly depends on the thickness of the ferromagnetic layer (inversely proportional to thickness)[33]. For the bottom layer, the PMA field overcomes the demagnetizing field to have net effective PMA. Therefore, the bottom layer has a perpendicular magnetic easy axis. However, the PMA value in the top layer is less than the demagnetizing field. Therefore, the top layer has an in-plane magnetic easy axis[33].

To evaluate the VCMA field, we measure the differential resistance (dV/dI) of the MTJ as a function of an external magnetic field along the y-axis (H_y) under various bias voltages (V_b) ranging from −0.4 to +0.4 V. A positive voltage means the bottom electrode has positive potential with respect to the top electrode of the MTJ.

The curves of normalized dV/dI at $V_b = -0.4$ V (red line) and +0.4 V (blue line) are plotted as functions of H_y in Fig. 1(b). At $\mu_0 H_y = -2.0$ T, the two curves show their minimum values after saturation, indicating that the magnetizations in both (top and bottom) CoFeB layers are along the negative y-axis. As H_y increases to zero, the curves of dV/dI under $|V_b| = 0.4$ V increase and reach maximum values at the zero magnetic field, indicating that the magnetization in the bottom CoFeB layer is almost aligned along the out-of-plane direction. When H_y turns to a positive value, the magnetization in the top CoFeB layer starts to align towards the positive y-axis. Then, the curves of dV/dI decrease with the increase in H_y for both bias voltages and reach minimum values again, indicating that the magnetizations of both CoFeB layers again lie along the in-plane direction (+y-axis).

The difference between the two curves in Fig. 1(b) is clear. The difference comes from the modulation of an interfacial PMA field (H_k) by V_b through the VCMA effect. From the difference in H_k due to the applied V_b, the

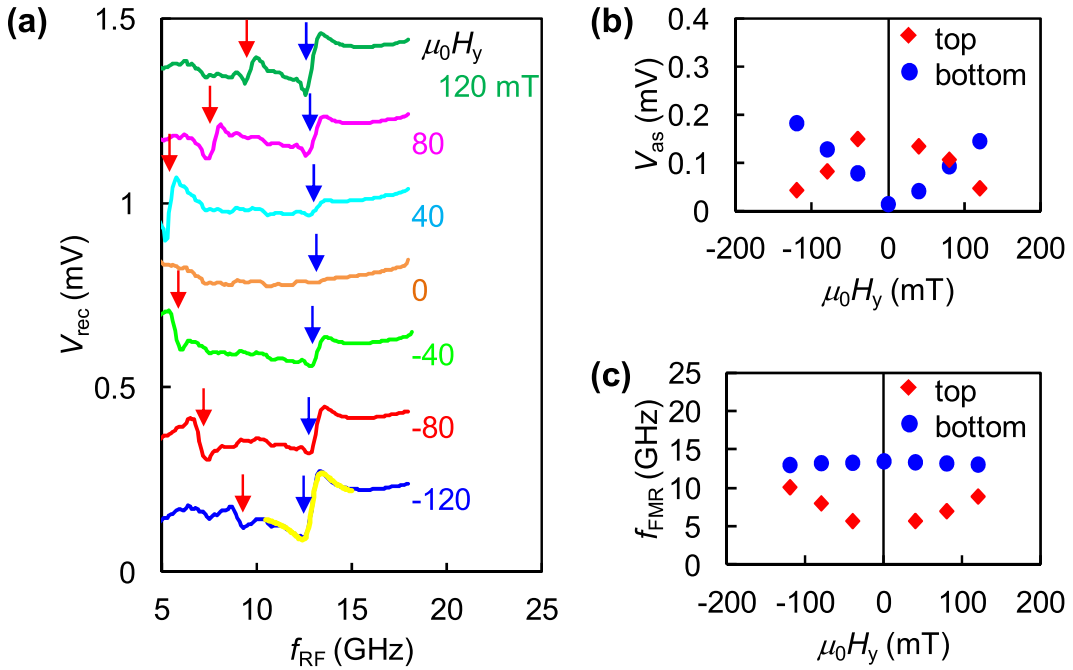

Figure 2. Experimental results of rectified voltage. (**a**) V_{rec} as function of f_{RF} with $V_{RF} = 0.4$ V at $\mu_0|H_y|$ of 0, 40, 80, and 120 mT. V_{rec} curves at different H_y are vertically offset by 0.25 mV. FMR peaks indicated by red arrows come from top CoFeB layer, and peaks indicated by blue arrows come from bottom CoFeB layer. Yellow line represents fitting curve obtained using Eq. (1). (**b**) Dependence of V_{as} on H_y. Red (blue) symbols represent V_{as} of top (bottom) layer. (**c**) Dependence of f_{FMR} on H_y. Red (blue) symbols represent V_{as} of top (bottom) layer.

magnitude of VCMA, *i.e.*, $\mu_0 \Delta H_k / V$, can be determined. We evaluate ΔH_k, which are defined by the difference between $H_k(V_b)$ and $H_k(0)$ (by using the method mentioned in pervious studies 24, 34), at $|V_b| = 0$, 0.2, and 0.4 V, and Fig. 1(c) plots ΔH_k as a function of V_b. The gradients of $\mu_0 \Delta H_k$ are different for positive and negative V_b. At positive (negative) V_b, $\mu_0 \Delta H_k / V_b$ is 127.1 (26.0) mT/V. The possible reason behind the difference between gradients under positive and negative V_b has been discussed[29,34]. According to these reports, the different thicknesses of the two CoFeB layers in the MTJs may show asymmetric dependence of PMA on positive and negative V_b.

Figure 2(a) shows the dependencies of V_{rec} on the excitation frequency (f_{RF}) at an amplitude of RF voltage $V_{RF} = 0.4$ V. A static magnetic field is applied along the *y*-axis ranging from −120 to +120 mT (see Methods). In this figure, each curve of V_{rec} artificially shifts by 0.25 mV vertically.

The curves of V_{rec} show two FMR peaks[35]. One of the FMR peaks shows a strong dependence of resonance frequency (f_{FMR}) on H_y (indicated by red arrows), whereas the other peak shows a slight change in f_{FMR} with H_y (indicated by blue arrows). The former peak corresponds to the FMR of the top CoFeB layer, whereas the latter peak corresponds to that of the bottom CoFeB layer.

The difference between the dependencies of f_{FMR} on H_y in the two layers can be explained as follows. The f_{FMR} of a ferromagnetic layer depends on the effective magnetic field of the layer. The effective field of the top CoFeB layer monotonically increases with $|H_y|$ due to the in-plane easy-axis of magnetization. On the other hand, the effective field of the bottom CoFeB layer does not vary significantly in the range of applied magnetic field due to the presence of strong PMA. In the case at $\mu_0|H_y| = 120$ mT, the magnetization of the bottom CoFeB layer tilts only up to 13° from the *z*-axis (Fig. 3(c)).

The line shapes of resonance peaks (Fig. 2(a)) in the bottom and top layers can be fitted by the sum of the symmetric and anti-symmetric Lorentzians given by[24,35,36]:

$$V_{rec} = \frac{V_s}{1 + (f - f_{FMR})^2/\sigma^2} + \frac{V_{as}(f - f_{FMR})/\sigma}{1 + (F - F_{FMR})^2/\sigma^2} \quad (1)$$

where V_s (V_{as}) is the symmetric (anti-symmetric) term of signal amplitude, and σ is the half width at half maximum. Here, V_s originates from the STT-induced FMR, whereas V_{as} comes from the FMR induced by modulation of the effective field through VCMA and field-like torque (FLT)[24,36,37].

Equation (1) fits the experimental resonance peaks quite well. Figure 2(a) shows an example of such fitting for V_{rec} at $\mu_0 H_y = -120$ mT for the bottom CoFeB layer (yellow line). According to the results of fitting, V_{as} is around ten times larger than V_s for both layers. Therefore, the contribution of VCMA torque is dominant over the STT because the contribution of the STT is too small to induce FMR due to the large resistance of the 2.0-nm-thick MgO barrier (current density is less than 1.0×10^6 A/m^2). Similarly, the FLT is also expected to be much smaller than VCMA torque[28].

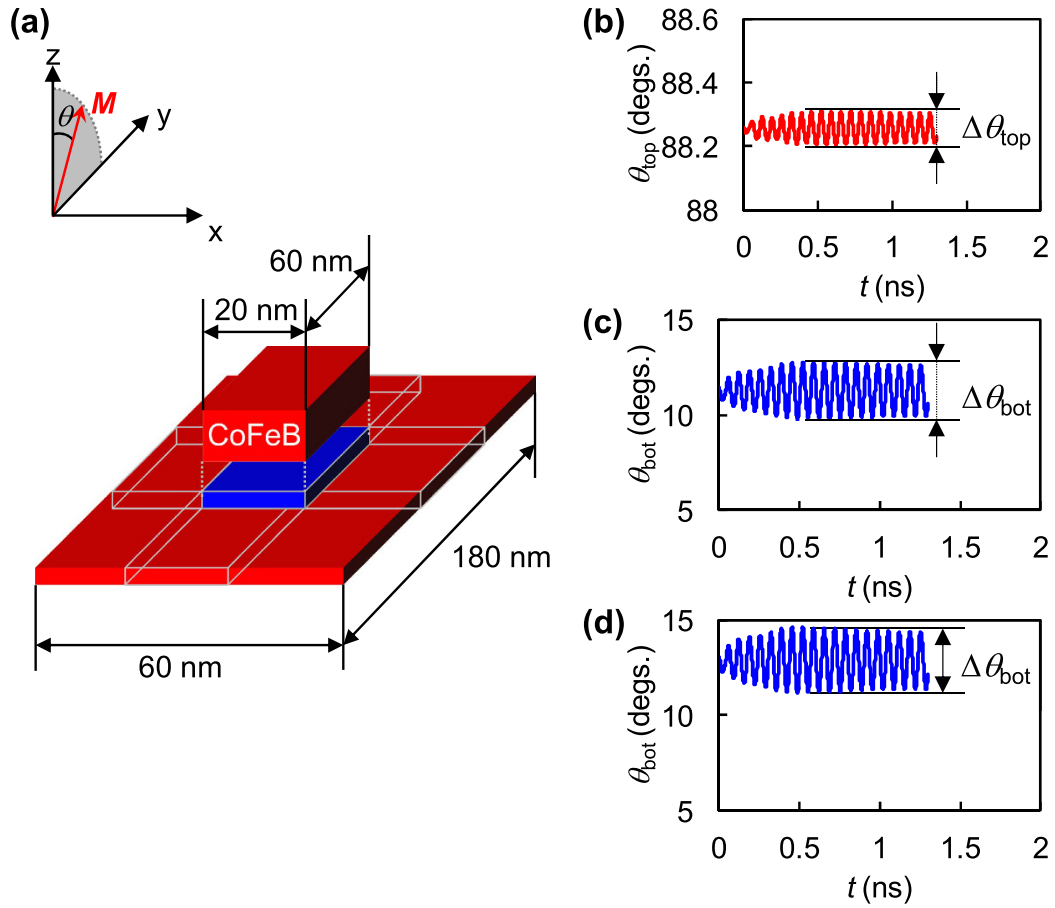

Figure 3. Schematic of model sample for micromagnetic simulations and simulation results. (**a**) Schematic illustration of model samples with top and bottom CoFeB layers. Blue indicates area where RF voltage is applied to bottom CoFeB layer. Coordinate system is also shown. (**b**,**c**) θ_{top} and θ_{bot} as functions of t under applied VCMA field of 30 mT and $f_{RF} = 15$ GHz for sample that includes both top and bottom CoFeB layers. (**d**) θ_{bot} as function of t under applied VCMA field of 30 mT and $f_{RF} = 15$ GHz for sample without top CoFeB layer. In simulations, offset field H_{offset} to H_{eff} is added for correcting zero point of VCMA on V_b.

Figure 2(b) shows the V_{as} of the top and bottom layers as functions of H_y. As shown in Fig. 2(b), the V_{as} of the top layer is maximum at $H_y = 0$ and decreases with $|H_y|$. This is because the equilibrium direction of the magnetization slightly tilts from the x-y plane at $H_y = 0$ due to the interlayer dipolar coupling and aligns toward the y-direction as H_y increases (see Fig. 3(b)). The small angle tilted from the x-y plane contributes to the magnetization motion in this case. Therefore, V_{as} strongly depends on the initial configuration of the magnetizations, *i.e.*, having a finite angle between the magnetization direction and z-axis at $H_y = 0$. In contrast, the V_{as} of the bottom layer is almost zero at $H_y = 0$ and increases monotonically with $|H_y|$. The reason for the V_{as} behaviour of the top and bottom layers is discussed in detail with the help of micromagnetic simulations in the last section of this report.

Figure 2(c) plots the f_{FMR} of the top and bottom layers obtained from the fitting as functions of H_y. As shown in Fig. 2(c), the f_{FMR} of the top layer increases with $|H_y|$, reflecting the increase in the effective field, as mentioned above. The f_{FMR} of the bottom layer slightly decreases as $|H_y|$ increases because of the weak dependence of the effective field on H_y in the out-of-plane magnetization configuration.

From the experiments, we find that the dependence of the magnitude of the magnetization motion on H_y is different between the top and bottom CoFeB layers. The results indicate that the amplitude of the magnetization motion in MTJs can be potentially controlled by the initial configuration of two magnetizations in the top and bottom magnetic layers.

The V_{rec} can be expressed as a time-averaged value of the product of oscillating magneto-resistance due to the precession of magnetization via the VCMA and RF tunnel current as[24,36]

$$V_{rec} = \langle R(t) I_{RF}(t) \rangle = \left\langle \frac{R}{1 + p^2 \cos\varphi(t)} \frac{V_{RF}}{R} \sin(2\pi f_{RF} t) \right\rangle \quad (2)$$

where R is the static resistance of an MTJ, p is spin polarization, and $\varphi(t)$ is the time-dependent relative angle between the magnetizations in the top and bottom CoFeB layers. The term $R(t) = R/(1 + p^2 \cos\varphi(t))$ represents the

time-dependent resistance due to oscillation of φ, and $I_{RF}(t) = V_{RF}\sin(2\pi f_{RF}t)/R$ represents the time-dependent tunnel current. As shown in Eq. (2), V_{rec} is represented by the time variation of φ when V_{RF} is applied. To obtain the magnetization motion of the top and bottom CoFeB layers through the time variation of φ, therefore, we conduct micromagnetic simulations based on the LLG equation of motion by taking into account the VCMA effect.

The LLG equation of motion is given by

$$\frac{d\mathbf{M}}{dt} = -\gamma\mathbf{M} \times \mathbf{H}_{eff} + \alpha\mathbf{M} \times \frac{d\mathbf{M}}{dt} \quad (3)$$

where the STT term can be ignored because of its small contribution in the MTJ. In this equation, **M** is magnetization, $\gamma = 1.7 \times 10^{-11}$ is the gyromagnetic ratio, $\alpha = 0.03$ is the Gilbert damping constant[33], and $\mathbf{H_{eff}}$ is the effective magnetic field. The effective field in the perpendicular direction $(H_{eff})_z = [H_k + \Delta H_k \sin(2\pi f_{RF}t)]\cos\theta$ includes contributions from H_k and the time-dependent modulation of the PMA field $\Delta H_k \sin(2\pi f_{RF}t)$ by applying V_{RF}. Equation (3) is numerically solved using the object-oriented micromagnetic framework (OOMMF) simulator[38].

The model samples for the simulations have top (with the in-plane magnetic easy axis) and bottom (with the perpendicular magnetic easy-axis) CoFeB layers separated by a distance of 2.0 nm (Fig. 3(a)) to mimic the experimentally measured MTJ with a 2.0-nm-thick insulating MgO layer (see Methods). The $\mu_0\Delta H_k$ is taken as 30 mT, which corresponds to the experimentally applied V_{RF} of 0.4 V. In all our simulations, a static magnetic field of 120 mT is applied along the *y*-axis.

The simulation results of the polar angles (angles with respect to the *z*-axis) of the magnetizations in the top and bottom CoFeB layers, θ_{top} and θ_{bot}, are plotted as functions of an elapsed time *t* when applying RF voltage with $f_{RF} = 15.0$ GHz in Fig. 3(b) and (c), respectively. In this case, the VCMA field is applied only to the area of the bottom CoFeB layer just below the top CoFeB layer (blue area in Fig. 3(a)). The θ_{top} is obtained from the averaged magnetization over the top CoFeB layer and θ_{bot} from the averaged magnetization over the blue area in the bottom CoFeB layer.

As shown in Fig. 3(b), at $t = 0$, the magnetization in the top CoFeB layer makes a small angle (~1.8°) with respect to the *x*-*y* plane due to the interlayer dipolar coupling with the bottom CoFeB layer. The magnetization of the bottom CoFeB layer is also tilted from the perpendicular direction by around 11° (Fig. 3(c)), reflecting the effect of the sum of H_y and interlayer dipolar coupling.

As *t* increases, the magnetization in the bottom CoFeB layer oscillates at a frequency of 15 GHz due to VCMA. The magnetization in the top CoFeB layer also oscillates despite the fact that VCMA is not taken into account in the simulation model and 15 GHz is not the resonance frequency of the top layer. These results indicate that a small amount of angular momentum of the bottom CoFeB layer is transferred to the top CoFeB layer due to the dynamic dipolar coupling between them while they are separated by a distance of 2.0 nm[39].

As shown in Fig. 3(b) and (c), $\Delta\theta_{top}$ and $\Delta\theta_{bot}$ are defined as amplitudes of oscillation angles of magnetizations in the top and bottom CoFeB layers, respectively. At $f_{RF} = 15.0$ GHz, $\Delta\theta_{bot} = 2.9°$ and $\Delta\theta_{top} = 0.1°$ are obtained. To confirm the magnitude of the transferred angular momentum, we also conduct a simulation by using a model sample with a bottom CoFeB layer only. Figure 3(d) plots θ_{bot} as a function of *t*. In this case, we obtain $\Delta\theta_{bot} = 3.4°$, which is larger than that in the sample with the top CoFeB layer. This result indicates that in our simulation model, the angular momentum is transferred from bottom to top CoFeB layers by more than 3% in angle equivalent. Similarly, the angular momentum induced in the excitation area (blue area in Fig. 3(a)) may also be transferred to the remaining area in the bottom CoFeB layer (red area in the bottom CoFeB layer in Fig. 3(a)).

We conduct the simulations at various f_{RF} at $\mu_0 H_y = 120$ mT using a model sample with the top and bottom CoFeB layers and plotted V_{rec} calculated from simulation results as a function of f_{RF} (Fig. 4(a)). Note that the VCMA field is applied only to the bottom CoFeB layer in this simulation.

The simulated V_{rec} reproduces the experimentally obtained FMR signal at 15.6 GHz from the bottom CoFeB layer, as shown in Fig. 2(a). However, the simulated resonance frequencies of the top and bottom CoFeB layers are larger than the experimental values due to the smaller dimensions of the model sample for simulation compared to the dimensions of the experimental sample[40]. The height of the resonance peak at around 10 GHz, which comes from the oscillation in the top CoFeB layer, is much smaller than that at 15.6 GHz, unlike the experimental results.

The possible reason for the small amplitude of the resonance peak at around 10 GHz is explained as follows. The simulated $\Delta\varphi$ (blue line), which is the oscillation amplitude of the relative angle between magnetizations of the top and bottom layers, is plotted as a function of f_{RF} together with $\Delta\theta_{top}$ (red line) and $\Delta\theta_{bot}$ (green line) in Fig. 4(b). Both $\Delta\varphi$ and $\Delta\theta_{bot}$ increase as f_{RF} increases and reach a maximum of around 4° when f_{RF} approaches f_{FMR} of 15.6 GHz. In the case of the top CoFeB layer, $\Delta\theta_{top}$ shows a maximum value of 0.2° at 10.2 GHz. This peak corresponds to the f_{FMR} of the top CoFeB layer, as shown in Fig. 2(a), which is generated by the transfer of angular momentum from the bottom CoFeB layer, although the $\Delta\theta_{top}$ is not large enough to reproduce the experimentally obtained peak.

The $\Delta\theta_{top}$ shows another peak (0.1°) at 15.6 GHz, which corresponds to the f_{FMR} of the bottom CoFeB layer. This peak is considered to be induced by the FMR mode of the bottom CoFeB layer. Therefore, we conclude that the top CoFeB layer with the in-plane magnetic easy axis can be excited by the transfer of angular momentum from the bottom CoFeB layer. However, the signal is much smaller than that of the experiment.

We also conduct a simulation by taking into account the VCMA in the top CoFeB layer. It is also possible to excite the top layer by VCMA, like the bottom layer[25], since the top CoFeB layer has an interfacial PMA of about 0.8 T ($< M_s$), and the magnetization of the top CoFeB layer makes a small angle with in-plane direction under the equilibrium (static) condition (Fig. 3(b)). To reproduce the V_{rec} signal from the top CoFeB layer at around 10.0 GHz, the VCMA in the top CoFeB layer is included in the simulations in addition to that in the bottom CoFeB layer.

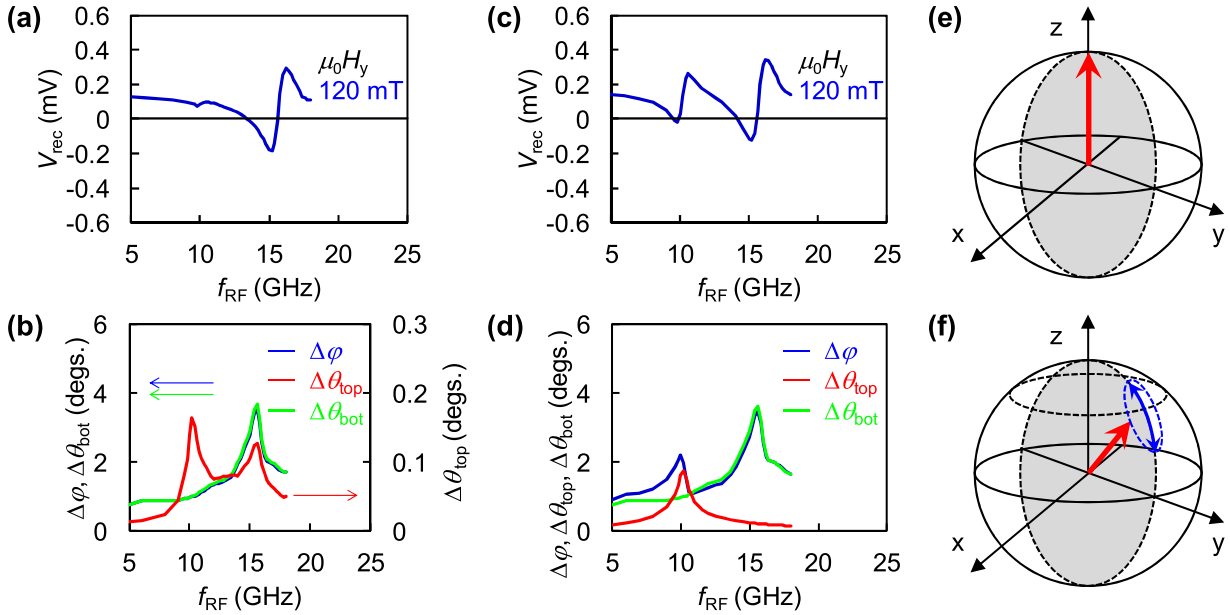

Figure 4. Micromagnetic simulation results and schematics of magnetization dynamics under VCMA. (**a**) Simulation results of V_{rec} as function of f_{RF} when VCMA is applied to bottom CoFeB layer. (**b**) $\Delta\varphi$ (blue line), $\Delta\theta_{top}$ (red line), and $\Delta\theta_{bot}$ (green line) as functions of f_{RF} when VCMA is applied to bottom CoFeB layer. (**c**) Simulation results of V_{rec} as function of f_{RF} when VCMA is applied to both top and bottom CoFeB layers. (**d**) $\Delta\varphi$ (blue line), $\Delta\theta_{top}$ (red line), and $\Delta\theta_{bot}$ (green line) as functions of f_{RF} when VCMA is applied to both top and bottom CoFeB layers. (**e**,**f**) Schematic figures of magnetization dynamics in bottom CoFeB layer without and with H_y, respectively.

The magnetization of the top CoFeB layer makes a small angle with the *x*-*y* plane. Because the VCMA field decreases in proportional to $\cos\theta$[25,41], the VCMA field applied to the top CoFeB layer must be smaller than that in the bottom CoFeB layer. In this model, the magnitude of the VCMA field applied to the top CoFeB layer is selected to be $\Delta H_k = -1.5$ mT, which is comparable to the estimated VCMA field considering factor $\cos\theta$. The ΔH_k in the z-direction is applied to the lower 1.0-nm region of the top CoFeB layer since VCMA is effective only at the interface area.

The simulation results of V_{rec} are plotted as a function of f_{RF} at $\mu_0 H_y = 120$ mT in Fig. 4(c). The simulated V_{rec} agrees well with the line shape of the experimentally obtained V_{rec} plotted in Fig. 2(a), showing two FMR peaks. Figure 4(d) illustrates the dependencies of $\Delta\varphi$ (blue line), $\Delta\theta_{top}$ (red line), and $\Delta\theta_{bot}$ (green line) on f_{RF}. In this figure, $\Delta\varphi$ shows two peaks, at 10.2 and 15.6 GHz, reflecting the FMR signals from the top and bottom CoFeB layers. In this simulation, therefore, the top layer is predominantly excited by VCMA, like the bottom layer.

Finally, we discuss the magnetization motion of the top and bottom CoFeB layers generated by RF voltage in detail. The V_{as} in the top CoFeB layer is maximum at $H_y = 0$ and decreases as $|H_y|$ increases. In the case of the top CoFeB layer, it is important to have a small angle between the magnetization direction and *x*-*y* plane for the magnetization motion, as mentioned above.

The V_{as} in the bottom CoFeB layer increases as $|H_y|$ increases in the magnetic-field range from −120 to +120 mT, while the V_{as} is almost zero at $H_y = 0$, as shown in Fig. 2(c). The dependence of V_{as} on H_y is consistent with the results presented in a previous study[25]. The possible reason for this behavior of V_{as} is explained as follows.

In the absence of H_y, the equilibrium direction of magnetization of the bottom CoFeB layer is in the *z*-axis. In this situation, the magnetization does not show apparent motion because VCMA corresponds to a modulation along the *z*-direction. As a result, the magnetization (red arrow) remains in the *z*-direction even under applied RF voltage, as shown in Fig. 4(e). In contrast, the equilibrium direction of the magnetization tilts toward the *y*-direction if H_y is applied. When RF voltage is applied, the VCMA field modulates the magnetization toward the *z*-direction. Therefore, the magnetization in this situation shows reciprocal motion in the *y*-*z* plane in addition to precessional motion, as shown in Fig. 4(f). We have also confirmed that the precessional amplitude (cone angle of precession) increases with the increase in $|H_y|$ in the range of our measurement (not shown), which is consistent with our experimental results.

Conclusion

We have investigated the magnetization motion in the two magnetic layers in MTJs under applied RF voltage by using both experimental measurements and micromagnetic simulations by taking into account VCMA. From the experiments, the dependence of the magnitude of the magnetization motion on H_y is different between the top and bottom CoFeB layers, and magnetization dynamics strongly depends on the initial angles of magnetizations with respect to the VCMA direction. From the simulation results, the magnetization motion in both the top and bottom CoFeB layers is induced by a combination of VCMA and transferred angular momentum, although the

magnetization direction of the two layers is different. Our results will have a large impact on understanding the mechanism of magnetization dynamics in MTJs excited by VCMA and developing voltage-controlled MTJs having PMA by controlling the initial angle between magnetizations and VCMA directions.

Methods

Sample fabrication. The film-stacking structure used in this study is prepared on a thermally oxidized Si(001) substrate by RF sputtering at room temperature at a base pressure of 10^{-9} Torr. The structure consists of the following layers (from the substrate side; nominal thicknesses in nanometres are stated in parentheses): Ta (5)/Ru (10)/Ta (5)/$Co_{20}Fe_{60}B_{20}$ (1.3)/MgO (2.0)/$Co_{20}Fe_{60}B_{20}$ (3.0)/Ta (5)/Ru (5). Rectangular shaped MTJs, as shown in Fig. 1(a), are fabricated by a combination of photolithography, Ar-ion milling, and RF sputtering in a multistep fabrication method. First, the top CoFeB layer of $2 \times 6\ \mu m^2$ is prepared by photolithography followed by Ar^+ ion milling down to the top MgO layer and subsequent deposition of Al_2O_3. In the second step, the bottom CoFeB layer with larger dimensions $40 \times 40\ \mu m^2$ is defined, keeping the former rectangular structure in the middle followed by Ar^+ ion milling down to the Si substrate. Third, 80-nm-thick insulator Al_2O_3 was deposited by sputtering everywhere except at the extremities of the top and bottom CoFeB layers. Finally, contacts made of Au (100 nm) are prepared by electron beam evaporation. The fabricated MTJs are annealed at 300 °C in vacuum under a perpendicular magnetic field of 600 mT for one hour.

Experimental measurement. The magnetization dynamics in CoFeB layers are excited by sending RF voltage through the capacitor port of a bias tee. The RF voltage (V_{RF}) produces an RF electric field (E_{RF}) at the interfaces of the top and bottom CoFeB/MgO layers. The E_{RF} modulates the interfacial PMA of both CoFeB layers. When the frequency of V_{RF} matches the f_{FMR} of any layer, the magnetization dynamics of that layer is excited. The magnetization dynamics produces an oscillatory TMR (depending upon the relative angle between the magnetizations of two layers) at the same frequency as that of the V_{RF}. The mixing of an oscillatory TMR and small RF tunnel current generates finite DC voltage (rectified voltage), which is measured using a voltmeter connected to the DC port of the bias tee.

Micromagnetic simulations. Two types of model samples are considered for the simulations. One has top and bottom CoFeB layers with thicknesses of 3.0 and 1.0 nm, respectively, as shown in Fig. 3(a). The mesh size is set to $2 \times 2 \times 1\ nm^3$. The two CoFeB layers are arranged 2.0 nm apart. The MTJs are downscaled to reduce the computation time. The lateral dimensions of the bottom CoFeB layer is $60 \times 180\ nm^2$, and those of the MgO and top CoFeB layers is $20 \times 60\ nm^2$. For the other model sample, we chose only a single CoFeB layer with a thickness of 1.0 nm and area $60 \times 180\ nm^2$. We adopt the anisotropy energy density of the bottom CoFeB layer in the perpendicular direction of $1.2\ MJ/m^3$, and the saturation magnetization M_s of 1.5 T, resulting in $\mu_0 H_k$ of around 500 mT. The ground state of magnetization is first prepared by applying a bias magnetic field along the *y*-axis. The dynamics is then excited by applying a sinusoidal RF magnetic field (ΔH_k) equivalent to a PMA field modulated by applied V_{RF} of 0.4 V. For the bottom layer, ΔH_k is selected as 30 mT (calculated from the experimental results shown in Fig. 1(c)). As the PMA is only modulated in the area of the bottom CoFeB layer underneath the top layer (blue area in Fig. 3(a)), ΔH_k is applied only to the blue area of the bottom CoFeB layer. In some simulations, the dynamics of the top CoFeB layer are also exited by a much smaller value of $\Delta H_k = -1.5$ mT along the *z*-axis. The reason behind this small value is explained in the main text.

References

1. Hosomi, M. *et al.* A novel nonvolatile memory with spin torque transfer magnetization switching: spin-ram. *IEDM Tech. Dig.* 459–462 (2005).
2. Kawahara, T. *et al.* 2 Mb SPRAM (spin-Transfer torque RAM) with bit-by-bit bi-directional current write and parallelizing-direction current read. *IEEE J. Solid-State Circuits* **43,** 109–120 (2008).
3. Kishi, T. *et al.* Lower-current and fast switching of a perpendicular TMR for high speed and high density spin-transfer-torque MRAM. *IEDM Tech. Dig*, 1–4 (2008).
4. Slonczewski, J. C. Current-driven excitation of magnetic multilayers. *J. Magn. Magn. Mater.* **159,** L1–L7 (1996).
5. Berger, L. Emission of spin waves by a magnetic multilayer traversed by a current. *Phys. Rev. B* **54,** 9353–9358 (1996).
6. Vlaminck, V. & Bailleul, M. Spin-wave transduction at the submicrometer scale: experiment and modeling. *Phys. Rev. B* **81,** 014425 (2010).
7. Bailleul, M. *et al.* Propagating spin wave spectroscopy in a permalloy film: a quantitative analysis. *Appl. Phys. Lett.* **83,** 972–974 (2003).
8. Kanai, S. *et al.* Electric field-induced magnetization reversal in a perpendicular-anisotropy CoFeB-MgO magnetic tunnel junction. *Appl. Phys. Lett.* **101,** 122403 (2012).
9. Worledge, D. C. *et al.* Spin torque switching of perpendicular Ta/CoFeB/MgO-based magnetic tunnel junctions. *Appl. Phys. Lett.* **98,** 022501 (2011).
10. Parkin, S. S. P. *et al.* Giant tunnelling magnetoresistance at room temperature with MgO (100) tunnel barriers. *Nat. Mater.* **3,** 862–867 (2004).
11. Yuasa, S. *et al.* Giant room-temperature magnetoresistance in single-crystal Fe/MgO/Fe magnetic tunnel junctions. *Nat. Mater.* **3,** 868–871 (2004).
12. Hayakawa, J. *et al.* Current-induced magnetization switching in MgO barrier based magnetic tunnel junctions with CoFeB/Ru/CoFeB synthetic ferrimagnetic free layer. *Jpn. J. Appl. Phys.* **45,** L1057–L1060 (2006).
13. Ikeda, S. *et al.* Tunnel magnetoresistance of 604% at 300 K by suppression of Ta diffusion in CoFeB/MgO/CoFeB pseudo-spin-valves annealed at high temperature. *Appl. Phys. Lett.* **93,** 082508 (2008).
14. Novosad, V. *et al.* Novel magnetostrictive memory device. *J. Appl. Phys.* **87,** 6400–6402 (2000).
15. Overby, M. *et al.* GaMnAs-based hybrid multiferroic memory device. *Appl. Phys. Lett.* **92,** 192501 (2008).
16. Ohno, H. *et al.* Electric-field control of ferromagnetism. *Nature* **408,** 944–946 (2000).
17. Chiba, D. *et al.* Electrical manipulation of magnetization reversal in a ferromagnetic semiconductor. *Science* **301,** 943–945 (2003).
18. Eerenstein, W. *et al.* Multiferroic and magnetoelectric materials. *Nature* **442,** 759–765 (2006).
19. Borisov, P. *et al.* Magnetoelectric switching of exchange bias. *Phys. Rev. Lett.* **94,** 117203 (2005).
20. Weisheit, M. *et al.* Electric field-induced modification of magnetism in thin-film ferromagnets. *Science* **315,** 349–351 (2007).

21. Chiba, D. *et al.* Magnetization vector manipulation by electric fields. *Nature* **455,** 515–518 (2008).
22. Nozaki, T. *et al.* Voltage-induced perpendicular magnetic anisotropy change in magnetic tunnel junctions. *Appl. Phys. Lett.* **96,** 022506 (2010).
23. Endo, M. *et al.* Electric-field effects on thickness dependent magnetic anisotropy of sputtered $MgO/Co_{40}Fe_{40}B_{20}/Ta$ structures. *Appl. Phys. Lett.* **96,** 212503 (2010).
24. Zhu, J. *et al.* Voltage-induced ferromagnetic resonance in magnetic tunnel junctions. *Phys. Rev. Lett.* **108,** 197203 (2012).
25. Nozaki, T. *et al.* Electric-field-induced ferromagnetic resonance excitation in an ultrathin ferromagnetic metal layer. *Nat. Phys.* **8,** 491–496 (2012).
26. Kanai, S. *et al.* Electric field-induced ferromagnetic resonance in a CoFeB/MgO magnetic tunnel junction under dc bias voltages. *Appl. Phys. Lett.* **105,** 242409 (2014).
27. Tulapurkar, A. A. *et al.* Spin-torque diode effect in magnetic tunnel junctions. *Nature* **438,** 339–342 (2005).
28. Kubota, H. *et al.* Quantitative measurement of voltage dependence of spin-transfer torque in MgO-based magnetic tunnel junctions. *Nat. Phys.* **4,** 37–41 (2008).
29. Shimabukuro, R. *et al.* Electric field effects on magnetocrystalline anisotropy in ferromagnetic Fe monolayers. *Phys. E* **42,** 1014–1017 (2010).
30. Duan, C. *et al.* Surface magnetoelectric effect in ferromagnetic metal films. *Phys. Rev. Lett.* **101,** 137201 (2008).
31. Nakamura, K. *et al.* Giant modification of the magnetocrystalline anisotropy in transition-metal monolayers by an external electric field. *Phys. Rev. Lett.* **102,** 187201 (2009).
32. Tsujikawa, M. & Oda, T. Finite electric field effects in the large perpendicular magnetic anisotropy surface Pt/Fe/Pt(001): a first-principles study. *Phys. Rev. Lett.* **102,** 247203 (2009).
33. Ikeda, S. *et al.* A perpendicular-anisotropy CoFeB–MgO magnetic tunnel junction. *Nat. Mater.* **9,** 721–724 (2010).
34. Nozaki, T. *et al.* Voltage-induced magnetic anisotropy changes in an ultrathin FeB layer sandwiched between two MgO layers. *Appl. Phys. Express* **6,** 073005 (2013).
35. Mizunuma, K. *et al.* Size dependence of magnetic properties of nanoscale CoFeB–MgO magnetic tunnel junctions with perpendicular magnetic easy axis observed by ferromagnetic resonance. *Appl. Phys. Express* **6,** 063002 (2013).
36. Sankey, J. C. *et al.* Measurement of the spin-transfer-torque vector in magnetic tunnel junctions. *Nat. Phys.* **4,** 67–71 (2008).
37. Wang, C. *et al.* Bias and angular dependence of spin-transfer torque in magnetic tunnel junctions. *Phys. Rev. B* **79,** 224416 (2009).
38. Donahue, M. J. & Porter, D. G. *OOMMF User's Guide, Version 1.2*, Interagency Report NISTIR 6376 (NIST, Gaithersburg, MD, 1999) at http://math.nist.gov/oommf/. (Accessed: 16th November, 2016).
39. Schneider, T. *et al.* Spin-wave tunnelling through a mechanical gap. *Europhys. Lett.* **90,** 27003 (2010).
40. Barman, A. *et al.* Magneto-optical observation of picosecond dynamics of single nanomagnets. *Nano Lett.* **6,** 2939–2944 (2006).
41. Hirayama, E. *et al.* Electric-field induced nonlinear ferromagnetic resonance in a CoFeB/MgO magnetic tunnel junction. *Appl. Phys. Lett.* **107,** 132404 (2015).

Acknowledgements

We would like to acknowledge M. Furushima for his technical supports as well as J. Hayakawa, O. Rousseau, P.E. Roy, and J. Wunderlich (Hitachi Europe Ltd.) for their fruitful discussions.

Author Contributions

Y.O. and H.T. supervised the study. K.M. wrote the manuscript. M.Y. and S.O. prepared samples and fabricated devices. K.M. and B.R. conducted the measurements. K.M. and S.Y. conducted the numerical simulations. S.Y., M.I. and Y.F. provided considerable help in the study. All authors analyzed the data, discussed the results, and commented on the manuscript.

Additional Information

Competing financial interests: The authors declare no competing financial interests.

How to cite this article: Miura, K. *et al.* Voltage induced magnetization dynamics in CoFeB/MgO/CoFeB magnetic tunnel junctions. *Sci. Rep.* **7**, 42511; doi: 10.1038/srep42511 (2017).

Publisher's note: Springer Nature remains neutral with regard to jurisdictional claims in published maps and institutional affiliations.